Biomass Combustion in a Fluidized-Bed System: An Integrated Model for Dynamic Plant Simulations

ARTICLE *in* INDUSTRIAL & ENGINEERING CHEMISTRY RESEARCH · JULY 2011

Impact Factor: 2.59 · DOI: 10.1021/ie200537m

I&EC research
Industrial & Engineering Chemistry Research

ARTICLE

pubs.acs.org/IECR

Biomass Combustion in a Fluidized-Bed System: An Integrated Model for Dynamic Plant Simulations

Vikranth Kumar Surasani,*[,†] Franka Kretschmer,[†] Patric Heidecke,[‡] Mirko Peglow,[†] and Evangelos Tsotsas[†]

[†]Thermal Process Engineering, Otto von Guericke University Magdeburg, Magdeburg, Germany

[‡]Virtual Development Training Center, Fraunhofer-IFF, Magdeburg, Germany

ABSTRACT: A model that can be used for dynamic simulation of fluidized-bed biomass combustion plants is presented. The model combines spatially concentrated (well-mixed) approaches for the fluidized bed and the ash separation cyclone with a one-dimensional plug-flow representation of the freeboard section. Simulation results are compared with steady-state experimental data for wood combustion in a laboratory-scale facility. Computed flue gas compositions are in good agreement with measured values, whereas some deviation is observed in fluidized-bed temperature. The integrated model provides reasonable accuracy at a high computational speed. Hence, it is appropriate, after coupling with a thermodynamic cycle, for real-time monitoring and control of distribution nets and electric grids supplied by various regenerative power sources. Possible model extension by a population balance for the fuel particles is briefly outlined.

1. INTRODUCTION

Increasing awareness of the depletion of fossil fuels and greenhouse gas emissions from conventional methods have made the generation of heat and power from biomass a top-priority research area in academia and industry. Biomass absorbs carbon dioxide during growth and releases it during combustion, making it CO_2-neutral; hence, biomass offers an attractive renewable alternative for power plants.[1] Biomass fuels include wood and woody waste, as well as a multitude of agriculture residues. A large number of different combustors/gasifiers[2,3] have been developed corresponding to the specific properties of typical fuels or ranges of fuels. The chemical, physical, and morphological properties of biomass fuels vary greatly, imposing different demands on the method of gasification/combustion. Thus, it is vital for biomass reactors to have fuel flexibility. Fluidized-bed (FB) technology combines such flexibility with economic and environmental advantages, and is therefore one of the most efficient and suitable among the proven combustion technologies for low-grade coals and a wide range of biomass.[2,4] Large contact area between the solids and the gas phase and efficient mixing in the fluidized bed favor isothermal conditions, which lead to better control of emissions and lower operating temperatures.

With the increasing number of renewable power generating plants in the electric grid, distribution net stability has become a crucial issue. Toward this end, model-based predictions of load influences from power plants based on renewable energy sources are necessary. Concerning FB combustion/gasification, a large number of mathematical modeling and simulation approaches can be found in the literature.[5,6] Although most of the literature refers to coal, there are no conceptual differences between the fuels (coal and biomass) with respect to model structure and mathematical description.[6] Many similarities exist as well between combustion and gasification in an FB, for instance, in fluid dynamics, devolatilization, oxidation of volatiles, oxidation/reduction of char and comminution. From this point of view, operating conditions and input feeds make the difference between combustion and gasification of coal or biomass. Meanwhile, the range of models published or implemented in commercial and open-source numerical codes is very wide, from computational fluid dynamics models (CFDMs) to black box models (BBMs). Computational fluid dynamics models provide three-dimensional, non-isothermal results that account for the complex reactive transport phenomena and the dynamics of the gas−solids system under turbulent conditions, for example, in a fluidized-bed combustion (FBC) plant. Black box models are much simpler, computing temperatures and gas compositions on the basis of mass and energy balances formulated for stationary conditions over the entire plant. A compromise between CFDMs and BBMs are so-called fluidization models (FMs), which avoid the details of gas−solids dynamics but still maintain multiphase patterns by means of semi-empirical correlations from standard literature.[7,8]

The choice of the model depends on the objectives and the experimental information available. In the present work, the goal was to provide simulations of biomass FBC plants those can be used for electric grid monitoring and stabilization. Such models must consider all significant parts of the plant in a dynamic way, and they must provide sufficiently accurate results in real time. Neither CFDMs nor BBMs fulfill these requirements, hence, a fluidization model (FM) has been adapted to represent the overall behavior of the biomass combustion plant. First, a specific bubbling fluidized-bed combustion facility with a 100 mm diameter fluidization vessel, denoted as BFBC 100, is described. Then, underlying assumptions for the model are discussed, and energy and mass conservation equations are presented for three parts of the plant, namely, the fluidized bed, freeboard, and cyclone. Finally, the sub-models are integrated, and simulation

Received: March 19, 2011
Accepted: July 11, 2011
Revised: June 2, 2011
Published: July 11, 2011

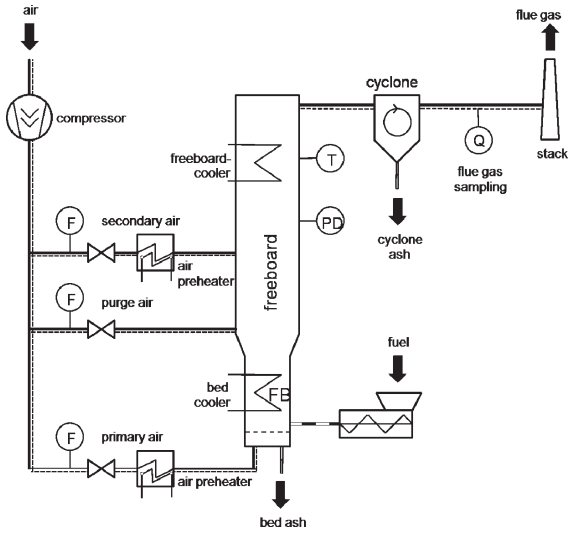

Figure 1. Flow sheet of the biomass fluidized-bed combustion plant.

results are compared with measurements available from the BFBC 100 facility. This article concludes by describing possible extensions of the presented FM with population balances that might contribute to better capturing particle-scale effects in the future.

2. BUBBLING FLUIDIZED-BED COMBUSTION PLANT

The experimental bubbling fluidized-bed combustor, BFBC 100, is located at Otto von Guericke University Magdeburg. Figure 1 presents a simplified process flowchart of the testing facility. The combustor has two sections, namely, the fluidized bed (FB) and the freeboard. The FB is operated with only the low excess pressure necessary to overcome the pressure loss of the combustor. Hence, the process can be referred to as atmospheric combustion. Quartz sand (0.8−1.2 mm) is used as the inert bed material for fluidization. Biomass fuel is transported into the FB by a screw feeder. Primary air is introduced through the perforated bottom plate in the FB, and secondary air is introduced through a lance fitted with nozzles in the freeboard. Electric air heaters that allow temperatures of 700 °C are present to preheat the primary and secondary air. In addition, air is introduced to purge two sight glasses. The cylindrical combustor has a total height (both FB and freeboard) of 4.24 m and a diameter of 100 mm in the bed region, which expands to 160 mm in the freeboard. The combustor is completely fabricated of heat-resistant stainless steel and has three layers of heat insulation.

The stationary BFBC 100 plant has a maximum thermal firing capacity of 15 kW. Flue gas is sampled between the cyclone and stack to continuously measure its composition and pollutant emissions. It is supplied to the analysis equipment through a heated line. Rosemount and Sick-Maihak gas analysis systems are used, thus making it possible to measure online flue gas compositions. Every test was followed by cyclone ash sampling to characterize the burnout of the fuel; the fuel's carbon content was analyzed.

3. MODELING

During combustion, with the gradual increase in temperature, every biomass particle undergoes a series of conversion processes: First drying and devolatilization, then oxidation of volatiles, and finally oxidation of char take place. Particles are affected by shrinkage and primary fragmentation as a consequence of thermal stresses, and internal pressure causes the release of volatiles. Secondary and percolation fragmentation and attrition of char take place during the char conversion process. Because of intense mixing, even spatial distribution of char and devolatilization can be assumed in the FB. The effects of fragmentation and attrition of fuel particles are neglected in the present model. Extensive reviews on the modeling of the thermochemical conversion of biomass (pyrolysis, combustion, and gasification) exist in the literature.[9]

Based on the internal transport of particles, the plant can be divided into three major parts: fluidized bed (FB), freeboard, and cyclone separator. First, biomass fuel reacts with primary air to form gaseous products in the FB, where inert material (sand) is used as a fluidization aid. Intense solid−solid and gas−solids interactions due to well-mixed conditions exist in the FB, which is a dense-phase system. Unburned biomass, char, and volatiles undergo combustion with the secondary air in the freeboard. Here, the gas content is high, and the interaction between the solids is negligible, which makes the freeboard a lean-phase system. In the cyclone separator, the formed particulates of ash and unburned char are separated from the hot gas stream. In the following subsections, the reaction mechanisms, basic assumptions of the three sub-models mass and energy balance equations, and integration of the sub-models to obtain the overall dynamic behavior of the plant are discussed.

3.1. Reaction Mechanisms. The reactions employed in the model are heterogeneous solid−gas reactions and homogeneous gas-phase reactions; see Table 1. Drying of the biomass is considered to be instantaneous. Char and volatiles compositions from pyrolysis of dry biomass (reaction R_1) are estimated based on experimental procedures of Wiest[10] and standard laboratory test methods DIN 51719[11] and DIN 51720.[12] In accordance with the experimental procedures[10−12] on the woody biomass used in the BFBC 100 plant, Tepper[13] established the hypothetical formula $C_6H_9O_4$ for the dry biomass. During the pyrolysis of dry biomass (reaction R_1), the produced char is not made of pure carbon, but rather has an elemental mass composition of 82.6% C, 4.3% H, and 1.31% O, equivalent to the hypothetical empirical formula $C_1H_{0.6}O_{0.12}$. Reactions R_1−R_5 are heterogeneous solid−gas reactions. The volatiles released from reaction R_1 undergo further reactions, namely, carbon monoxide combustion (R_6), water−gas shift reaction (R_7), methane partial oxidation (R_8), and hydrogen combustion (R_9). The kinetic parameters and rate expressions used were obtained from the references cited in Table 1.

3.2. Assumptions. Because the fluidized bed (FB) is operated only at low excess pressure to counteract the pressure drop, the system is referred to as an atmospheric FB. The main assumptions in the modeling of the FB are as follows:

(1) The FB sub-model is of zero dimension, with the assumption that the fluidized bed (FB) behaves like a continuous stirred tank reactor (CSTR) with respect to both the solids and the gas.
(2) The model includes only the emulsion phase; that is, bubble formation is not considered explicitly.
(3) Drying of biomass is instantaneous, and the heat loss due to evaporation of water being considered in the energy balance equations.
(4) Pyrolysis of biomass takes place without significant consumption or release of energy (the reaction is neither exothermic nor endothermic).

Table 1. Reactions Involved in the Model and Literature Sources from Which the Kinetic Parameters Were Obtained

type	mechanism
R_1, pyrolysis[13]	$C_6H_9O_4(s) \rightarrow 2.54C_1H_{0.62}O_{0.12}(s) + 2.19CO(g) + 0.24CO_2(g) + 1.03CH_4(g) + 0.63\ H_2(g) + 1.02H_2O(g)$
R_2, char combustion[14]	$C_1H_{0.62}O_{0.12}(s) + 1.095O_2(g) \rightarrow CO_2(g) + 0.31H_2O(g)$
R_3, water−gas reaction[14]	$C_1H_{0.62}O_{0.12}(s) + 0.88H_2O(g) \rightarrow CO(g) + 1.19H_2(g)$
R_4, methane formation[14]	$C_1H_{0.62}O_{0.12}(s) + 1.82H_2(g) \rightarrow CH_4(g) + 0.12H_2O(g)$
R_5, Boudouard reaction[15]	$C_1H_{0.62}O_{0.12}(s) + CO_2(g) \leftrightarrow 2CO(g) + 0.12H_2O(g) + 0.19H_2(g)$
R_6, carbon monoxide oxidation[16]	$CO(g) + {}^1/_2O_2(g) \rightarrow CO_2(g)$
R_7, water−gas shift reaction[17]	$CO(g) + H_2O(g) \leftrightarrow CO_2(g) + H_2(g)$
R_8, methane partial oxidation[18]	$CH_4(g) + {}^3/_2O_2(g) \rightarrow CO(g) + 2H_2O(g)$
R_9, hydrogen oxidation[19]	$H_2(g) + {}^1/_2O_2(g) \rightarrow H_2O(g)$

Table 2. Mass and Energy Balance Equations for the Sub-models of a Fluidized-Bed Biomass Combustion Plant

plant section	phase	mass/momentum balance		energy balance	
fluidized bed	gas	$\frac{dM_{j,g}}{dt} = \dot{M}_{j,g,in} - \frac{1}{\tau_g}M_{j,g} + \sum_{i=1}^{Nr}\nu_{ij}R_i\tilde{M}_j$	(1)	$\frac{dH_g}{dt} = \dot{H}_{g,in} - \dot{H}_g + \dot{H}_{Net} + \sum_{i=1}^{Nr}\Delta H_{r,i}(T_g)R_i + \dot{Q}_{pg} - \dot{Q}_{loss}$	(3)
	solid	$\frac{dM_{j,p}}{dt} = \dot{M}_{j,p,in} - \frac{1}{\tau_p}M_{j,p} + \sum_{i=1}^{Nr}\nu_{ij}R_i\tilde{M}_j$	(2)	$\frac{dH_p}{dt} = \dot{H}_{p,in} - \dot{H}_p - \dot{H}_{Net} + \sum_{i=1}^{Nr}\Delta H_{r,i}(T_p)R_i - \dot{Q}_{evp} - \dot{Q}_{pg}$	(4)
freeboard	gas	$\frac{\partial M_{j,g,k}}{\partial t} = -\frac{\partial(v_{g,k}M_{j,g,k})}{\partial z} + \sum_{i=1}^{Nr}\nu_{ij}R_{i,k}\tilde{M}_j$	(5)	$\frac{\partial H_{g,k}}{\partial t} = -\frac{\partial(v_{g,k}H_{g,k})}{\partial z} + \sum_{i=1}^{Nr}\Delta H_{r,i,k}(T_{g,k})R_{i,k} - \dot{Q}_{loss,k}$	(7)
		$\frac{\partial(v_{g,k}M_{g,k})}{\partial t} = -\frac{\partial(v_{g,k}{}^2M_{g,k})}{\partial z}$	(6)		
cyclone	gas	$\dot{M}_g = \rho_g v_{g,cyc}A_{cyc,out}$	(8)	$\frac{dH_g}{dt} = \dot{H}_{g,cyc,in} - \dot{H}_{g,cyc,out} - \dot{Q}_{loss,cyc}$	(9)

(5) The solids transition from the FB to the freeboard is modeled without consideration of the particle size dependence of elutriation and entrainment phenomena.

The second sub-model for the freeboard involves the following assumptions:

(1) The freeboard is represented by a one-dimensional model with plug-flow conditions.
(2) Solid-phase transport and reactions (i.e., the heterogeneous solid−gas reactions R_1−R_5) are neglected in the system.
(3) Only homogeneous gas-phase combustion reactions (reactions R_6−R_9) are considered in this sub-model.

The third submodel represents the unit operation of solid−gas separation in the cyclone with the following assumptions:

(1) Reactions in the gas phase are neglected completely.
(2) Incompressible-flow conditions are applied.
(3) Considering the cyclone as a CSTR, the energy balance equation is formulated with the exit flue gas temperature.

3.3. Mass and Energy Balances. In the FB submodel, both homogeneous (gas−gas) and heterogeneous (gas−solids) chemical reactions are considered (see Table 1). Energy balance equations are expressed separately for the gas, the inert sand, and the fuel particles, incorporating heat-transfer coefficients between solids and gas. Based on the assumptions described in section 3.1, the heat and mass balance equations listed in Table 2 are obtained. Equations 1−4 represent the component mass and the energy balances of the well-mixed FB submodel, whereas eqs 5−7 represent the mass, momentum, and energy balances for the gas phase in the freeboard submodel.

The component mass balances in the gas phase for the FB sub-model is expressed by eq 1, where $M_{j,g}$ is the mass of component j in the gas phase, $\dot{M}_{j,g,in}$ is the inlet mass flow rate of the component, R_i is the rate of reaction i, ν_{ij} is the stoichiometric coefficient of component j in reaction i, and $\tilde{M}_j$ is the molecular weight of component j. The component mass balances for the fuel particles (biomass and char) are given by eq 2. Here, $M_{j,p}$ represents the mass of component j in the particle phase, and $\dot{M}_{j,p,in}$ the inlet mass flow rate of component j. The residence times of gas and fuel particles in the FB, denoted by τ_g and τ_p, respectively, are approximated by taking the ratio of the reactor volume not occupied by inert material to the inlet volume flow rate of the considered phase

$$\tau_g = \frac{V - (1-\varepsilon_{fix})V_{fix}}{\dot{V}_{g,in}} \quad (10)$$

$$\tau_p = \frac{V - (1-\varepsilon_{fix})V_{fix}}{\dot{V}_{p,in}} \quad (11)$$

Here, V is the total volume of the reactor, and V_{fix} and ε_{fix} are the volume and porosity, respectively, of the fixed bed of inert sand. The inlet volumetric flow rates of gas and fuel particles are denoted by $\dot{V}_{g,in}$ and $\dot{V}_{p,in}$, respectively.

Separate energy balances are employed for gas, inert sand, and fuel particles by incorporating the heat and mass transfer between the solids (fuel and sand) and the gas phase. The total energy balance for the gaseous phase in the FB combustor can be written as in eq 3 (see Table 2). In the gas phase, H_g is the

Table 3. Closure Equations for the Energy Balance in eqs 3, 4, and 12 over Gas Phase, Fuel, and Sand Particles

enthalpy content (J)	$H_g = \sum_j^{Nc_g} M_{j,g} c_{p,j,g} (T_g - T_{ref})$	(13)
	$H_p = \sum_j^{Nc_p} M_{j,p} c_{p,j} (T_p - T_{ref})$	(14)
	$H_s = M_s c_{p,s} (T_s - T_{ref})$	(15)
enthalpy flow rate (J/s)	$\dot{H}_{j,g} = \frac{1}{\tau_g} \sum_j^{Nc_g} M_{j,g} c_{p,j,g} (T_g - T_{ref})$	(16)
	$\dot{H}_{j,p} = \frac{1}{\tau_p} \sum_j^{Nc_p} M_{j,p} c_{p,j,p} (T_p - T_{ref})$	(17)
reaction enthalpy (J/mol)	$\Delta H_{r,i}(T) = \Delta H^0_{r,i}(T_{ref}) + \sum_{j=1}^{Nc} \nu_{ij} c_{p,j} \tilde{M}_j (T - T_{ref})$	(18)
net flow enthalpy (J/s)	$\dot{H}_{Net} = \sum_j^{Nc_g} \left[\left(\sum_{i=1}^{Nr} \nu_{ij} R_{i,p} \right) \tilde{M}_{j,g} c_{p,j,g} \right] (T_p - T_g)$	(19)
heat loss due to drying (J/s)	$\dot{Q}_{evp} = \dot{M}_{H_2O,in} [c_{p,l,H_2O} (T_{evp} - T_{p,in}) + \Delta H_{evp,H_2O} + c_{p,g,H_2O} (T_g - T_{evp})]$	(20)
heat exchange (J/s)	$\dot{Q}_{p\,or\,s,g} = A_{surf,p\,or\,s} \alpha_{g,p\,or\,s} (T_{p\,or\,s} - T_g)$	(21)
heat loss (J/s)	$\dot{Q}_{loss} = A_{surf,FB} \alpha_{eff} (T - T_{ambient})$	(22)

enthalpy content, $\dot{H}_{g,in}$ is the inlet enthalpy flow rate, $\dot{H}_g$ is the outlet enthalpy flow rate, and $\dot{Q}_{loss}$ is the heat loss through the wall. Similarly, for the total energy balance on the fuel particles (p) in eq 4, H_p is the enthalpy content of the particles, $\dot{H}_{p,in}$ is the inlet enthalpy flow rate, and $\dot{H}_p$ is the outlet enthalpy flow rate. The heat loss due to evaporation of water contained in the biomass is accommodated in eq 4 by the term $\dot{Q}_{evp}$. Finally, $\dot{Q}_{pg}$ is the heat flow rate from fuel particles to the gas phase, and $\dot{H}_{Net}$ is the enthalpy flow rate related to the change of phase of components due to heterogeneous reactions (the so-called net flow). The total energy balance on the inert sand can be written as

$$\frac{dH_s}{dt} = -\dot{Q}_{sg} - \dot{Q}_{loss} \quad (12)$$

where $\dot{Q}_{sg}$ is the heat-transfer rate from inert sand to the gas phase.

Table 3 expands terms contained in the energy balances in eqs 3 and 4. Equations 13−15 represent the enthalpy contents of individual phases (gas, fuel particles, and sand, respectively) in the FB. Equations 13 and 14 can also be used to calculate inlet enthalpy flow rates by replacing the masses of gas and fuel particles with the respective inlet mass flow rates. Equations 16 and 17 express the outlet enthalpy flow rates for gas and biomass, respectively. They are based on the assumption of CSTR behavior, according to which state variables in the system have the same value as at the outlet. Reaction enthalpies are calculated using eq 18; they are temperature-dependent and vary dynamically in the model. In the heterogeneous reactions involved (R_2−R_5), the fuel particles consume some gaseous components and release others. During this process, there is a net mass flow of gaseous components from the particle phase to the gas phase; enthalpy transfer due to the net flow of gaseous components can be calculated using eq 19. Because drying is assumed to be instantaneous, the energy consumed during this process is considered as a sink term in the energy balance equation of the particle phase (eq 4), calculated by means of eq 20.

According to previous investigations,[20] when both the solids and gas are assumed to be perfectly mixed in a fluidized bed, then equations based on single-particle behavior can be used to calculate particle-to-gas heat-transfer coefficients. Here, a popular equation of this type developed by Gnielinski was applied.[20,21] First, the particle Nusselt number

$$Nu_p = 2 + \sqrt{Nu_{lam}^2 + Nu_{tur}^2} \quad (23)$$

is computed from laminar and turbulent contributions

$$Nu_{lam} = 0.664 Re_p^{1/2} Pr^{1/3} \quad (24)$$

$$Nu_{tur} = \frac{0.037 Re_p^{0.8} Pr}{1 + 2.443 Re_p^{-0.1} (Pr^{2/3} - 1)} \quad (25)$$

where Pr is the Prandtl number and Re is the Reynolds number, defined as $c_{p,g}\mu_g/\lambda_g$ and $\rho_g v_g d_p/\nu_g$, respectively. Subsequently, the FB Nusselt number is obtained by multiplication with the empirical factor f_a, which depends on the porosity of the fluidized bed

$$Nu_{FB} = Nu_p f_a \quad (26)$$

$$f_a = 1 + 1.5(1 - \varepsilon_{FB}) \quad (27)$$

Finally, the particle-to-gas heat-transfer coefficients are calculated and inserted into eq 21, which is applied to both the fuel particles and the sand.

The heat loss through the wall is calculated by eq 22, where the effective heat-transfer resistance ($1/\alpha_{eff}$) is the sum of the conductive heat-transfer resistances of the wall and insulation and the convective heat-transfer resistances in the FB and air. The reference temperature, T_{ref}, is equal to the ambient temperature of 20 °C.

The one-dimensional plug-flow model for the freeboard is represented by eqs 5−7. The freeboard is subdivided into a

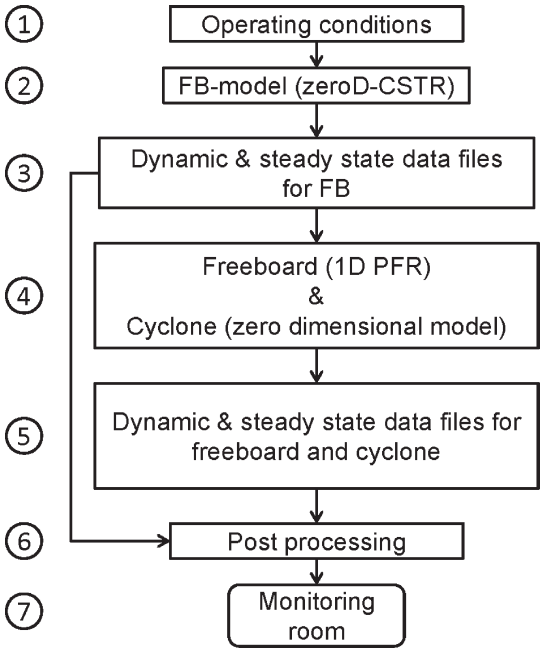

Figure 2. Flowchart representing the integration of sub-models for obtaining dynamic/steady-state simulation data of power plant operation.

number of control volumes that are denoted by the index k (45 control volumes were used in the present simulations), and the equations are solved simultaneously in every control volume (k). Because of volume changes accompanying gas-phase reactions, the flow velocity, $v_{g,k}$, can change along the freeboard (eq 6). The equations are closed by the same definitions of gas enthalpy and reaction enthalpy as in the FB (eqs 13 and 18, respectively); only gas-phase reactions are taken into account in the calculation of the reaction enthalpy. The heat loss in the freeboard is obtained by applying a modified version of eq 22 to every control volume. The same equation provides the heat loss from the cyclone. Modeling of the cyclone (eqs 8 and 9) is otherwise very simple, because reactions are neglected and the flow is considered to be well-mixed and incompressible.

3.4. Integration of Sub-models. The plant model is formed by integration of the sub-models for the fluidized bed, freeboard, and cyclone. This process of integration is explained in the flow sheet of Figure 2. Because heat and mass flows are unidirectional (i.e., from the fluidized bed to the freeboard to the cyclone) and the size dependence of fuel particle elutriation and entrainment is not considered, one-way coupling of the sub-models as shown in Figure 2 is sufficient to simulate plant behavior. Each event in the coupling process is numbered on the left-hand side of the figure. In step 1, all of the geometric and operating parameters are supplied to the model. In step 2, using the operating conditions, the FB model is solved by application of eqs 1−4. Data obtained in step 2 is stored as dynamic data files in step 3. From there, information is supplied to the post-processing step 6 and to the sub-models of the freeboard and the cyclone in step 4. Equations 5−9, which represent the submodels of the freeboard and cyclone, are solved simultaneously in step 4, and the dynamic data obtained in step 4 are stored in step 5 for the post processing (step 6). The idea behind the simulation is to supply all of the dynamic data obtained in steps 3 and 5 to a monitoring room. Such a monitoring room collects data from all power plants connected to a distribution net. In this way, it enables one to visualize the state of the electrical net, assess the evolution of this state in time, derive stable conditions, and identify decisions about the operational capacity of individual power providers that would serve overall net stability.

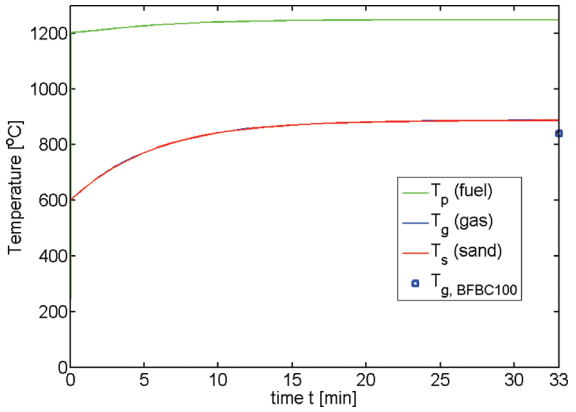

Figure 3. Evolution of the temperatures of the gas, inert sand, and fuel particles in the FB.

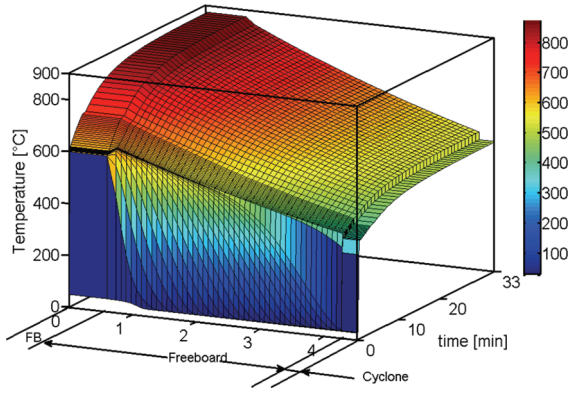

Figure 4. Dynamic evolution of the spatial temperature profiles in the BFBC 100 plant.

4. SIMULATION RESULTS AND VALIDATION

The integrated model was applied to the already described bubbling fluidized-bed combustor plant BFBC 100. The simulation results presented here are for a thermal firing capacity of 6.1 kW, which matches a fuel feed rate of 1.28 kg/h at room temperature. The fuel feed was woody biomass of 1 mm mean particle diameter consisting of 46.37% carbon (C), 6.17% hydrogen (H), 0.10% nitrogen (N), 38.41% oxygen (O), 0.06% sulfur (S), 0.24% ash, and 8.65% water (H_2O), with volatile matter comprising 76.52% by weight of the raw fuel. Primary air at 50 °C at a volume flow rate of 11 m^3/h was supplied to the FB, and no secondary air was used in the freeboard.

The obtained dynamic temperature profiles of fuel particles, sand, and gas in the FB are plotted in Figure 3. Because of intense gas−solids mixing in FB, the inert sand and the gas phase exhibit nearly equal temperatures. The curves representing the sand temperature (T_s) and the gas temperature (T_g) are thus almost identical and are superimposed in Figure 3. The gas temperature at the exit of the FB is practically equal to the bed temperature. This confirms the existence of nearly isothermal conditions in the

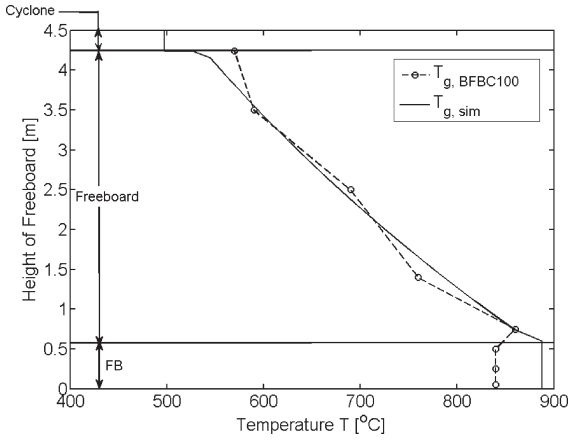

Figure 5. Measured and simulated steady-state gas temperature profiles in the BFBC 100 plant.

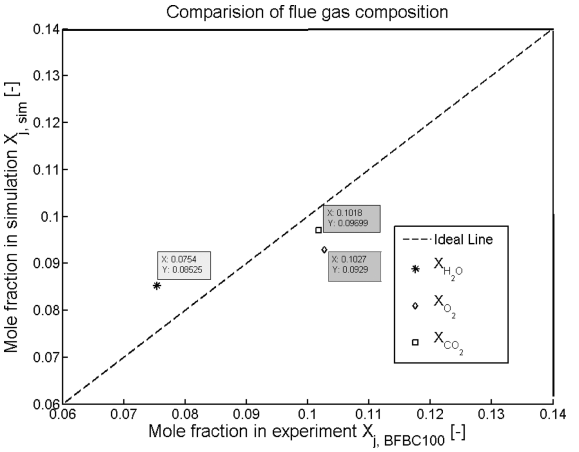

Figure 6. Comparison of simulated and experimental results for flue gas composition.

fluidized-bed region in accordance with the literature.[22] After the attainment of steady state, the calculated and measured gas temperatures are relatively close to each other. However, the fuel particles stay at much higher temperatures, because of the heat release by heterogeneous reactions. The gap between the gas and fuel temperatures might decrease with an increase in the moisture content of the biomass feed.

Figure 4 shows the dynamic evolution of the gas-phase temperature profiles over the height of the plant. The initial temperature of the sand was 600 °C. As soon as the fuel feed entered the bed, devolatilization took place under high-temperature conditions. With the immediate availability of oxidizing agent in the primary air, combustion of volatiles released heat. Furthermore, the intense mixing of gas and solids in the FB assured a uniform temperature of the bed (sand and gas phase; see Figure 3). Because of the processes of devolatilization and volatile combustion, as well as the well-mixed conditions, the temperature of the bed was self-sustained. This can be seen from Figures 3 and 4. Initially, gas in the FB was at room temperature. However, the gas temperature increased to approximately 600 °C (initial condition for the temperature of sand) in a very short period of time. With the combustion of char and volatiles, the temperature of the bed increased further and reached a steady state. The released gases flowed from the FB into the freeboard section, where any unburned volatiles underwent further combustion. Gas temperature profiles obtained with the assumed one-dimensional plug-flow model of the freeboard and the zero-dimensional representation of the cyclone are included in Figure 4.

The simulated gas temperature profile with plant height under steady-state conditions is compared with experimental results from the BFBC 100 plant in Figure 5. Concerning the fluidized bed, one can see that the difference in temperature between simulation and experiment, which appears to be small in Figure 3, is (with temperatures of approximately 890 °C according to the simulation and approximately 840 °C measured) not insignificant. Additionally, the simulated and measured temperature profiles show opposite behaviors at the interface between the FB and freeboard. The simulation shows a monotonic decrease in temperature along the entire freeboard height, whereas in the experiment, a certain increase in temperature took place over a few centimeters after the entry of the freeboard, followed by the expected decrease in temperature over the remaining height. This phenomenon is mainly due to further combustion of not only volatiles but also entrained char at the entrance of the freeboard, with the release of heat being dominant enough to overcome heat losses. Such a peak temperature in the freeboard cannot be observed in the simulation because heterogeneous reactions in the freeboard are not considered in the present model. Moreover, distributions of fuel particle size and density are not described in the fluidized bed, although they do have an influence on the fuel FB residence time and entrainment. The simulated and measured flue gas compositions are compared in Figure 6. The agreement is relatively good, with some overprediction of the mole fraction of water vapor and underprediction of the mole fractions of oxygen and carbon dioxide.

5. CONCLUSIONS AND OUTLOOK

In this article, a mathematical model for biomass combustion in fluidized-bed system is presented. It is an integrated model that consists of sub-models for the zero-dimensional FB, the one-dimensional plug-flow freeboard, and the zero-dimensional cyclone, as explained in section 3. The modeling strategy allows simulation of plants of any capacity, from the laboratory scale to the industrial scale. Such simulations can be used for feasibility and conceptual studies during the development of industrial facilities. On the other hand, with the presented approach, outlet mass flow rates and temperatures can be predicted in operating time in a real plant. Consequently, when combined with a thermodynamic cycle, the model can supply electric output parameters in real time. This feature of the model makes it possible to assess the influence that a number of biomass-based FB power plants of varying capacities would have on a distribution net. Therefore, this model can be combined with an electric grid model to predict load fluctuations and support monitoring and control. In the present article, validation was provided by data from only one experimental run in a laboratory-scale plant (BFBC 100). Current work aims at expanding the basis of available data to more laboratory-scale runs, as well as to experiments at the pilot and industrial scales (using plants with maximum firing capacities of 150 kW and 3.5 MW, respectively).

The presented model provides a basis for consideration of more physical effects mainly divided into two categories. First is the fuel particle behavior during the combustion. To accurately capture this behavior, eq 2 of the fluidized-bed sub-model should be replaced by a population balance equation for the fuel

particles. A population balance describes how the physical and chemical changes during drying, devolatilization, and char combustion contribute to changes in the fuel particle properties, namely, the size d_p and mass M_p (or size and density). It has the general form

$$\frac{\partial n_m}{\partial t} = \sum -\frac{\partial (G_L n_m)}{\partial \xi_L} + \ldots, \quad G_L = \frac{d\xi_L}{dt} = f(M_p, d_p, k) \tag{28}$$

where G_L is a growth term that represents the rate of change of particle property ξ_L, either mass or particle size. It can be correlated with the considered properties and the rate coefficient k, which is the sum of the individual rate coefficients from drying, devolatilization, and char combustion. Because all three processes occur simultaneously in the high-temperature FB, k plays a major role in the model for the exact evolution of volatile fractions and outlet temperatures. Notably, k varies among particle groups with different sizes and different densities. Thermogravimetric analysis is currently conducted to identify particle-size-dependent devolatilization kinetic parameters[23] for population balance modeling. The second category concerns the influence of the fluid-dynamic behavior of the bed on the fuel particles. This refers to the presence of bubbles (neglected here) and specifically to the influence of bubble eruptions on the transport (entrainment) of fuel particles from the FB into the freeboard section. Due to the presence of a size distribution, smaller fuel particles with a lower terminal fall velocity will be preferentially elutriated. With the inclusion of elutriation and entrainment processes due to bubbling and particle size distribution, the model would be able to predict more accurate temperatures in the FB. These effects can be implemented as future work by incorporating semiempirical correlations of the elutriation rate[24] and entrainment flux[25] into eq 28.

Upgrades to the described model are expected to provide more realistic flue gas compositions and temperature profiles for fluidized-bed biomass combustion plants, but they might also jeopardize the present advantage of fast, real-time computation. Consequently, it might be necessary to develop new concepts for preparing the results of complete simulations for electric network use.

AUTHOR INFORMATION

Corresponding Author

*Tel.: +1 814 863 2927. E-mail: vks10@psu.edu.

ACKNOWLEDGMENT

Financial support of this work by the German Federal Ministry of Education and Research (BMBF) is gratefully acknowledged.

NOMENCLATURE

A = area (m^2)
c_p = specific heat capacity under constant pressure [J/(kg K)]
d = diameter (m)
f_a = empirical factor
G = growth rate (kg/s or m/s)
$H|$ = enthalpy content (J)
$\dot{H}$ = enthalpy flow rate (J/s)
ΔH_r = reaction enthalpy (J/mol)
ΔH_{evp} = evaporation enthalpy (J/kg)
k = rate coefficient of reaction (of order n) ($mol^{1-n}\ m^{3(n-1)}\ s^{-1}$)
M = mass (kg)
$\dot{M}$ = mass flow rate (kg/s)
$\tilde{M}$ = molecular weight (kg/kmol or g/mol)
n = number of particles
$\dot{Q}$ = heat-transfer rate (J/s)
R_i = rate of reaction i (mol/s)
t = time (s)
T = temperature (K or °C)
V = volume (m^3)
$\dot{V}$ = volumetric flow rate (m^3/s)
v = velocity (m/s)
X = mole fraction
z = height (m)

Greek Letters

α = heat-transfer coefficient [$W/(m^2\ K)$]
ε = porosity
λ = thermal conductivity [W/(m K)]
μ = viscosity (N s/m^2)
ν = stoichiometric coefficient
ρ = density (kg/m^3)
τ = residence time (s)

Subscripts/Superscripts/Symbols

cyc = cyclone
eff = effective
evp = evaporation
FB = fluidized bed
fix = fixed bed of sand
g = gas
i = index of reactions
in = inlet
j = index of components
k = index of control volumes
L = index of properties (mass or particle size)
l = liquid
loss = heat loss
m = index of particle groups
Nc = number of components
Nr = number of reactions
Net = net flow
out = outlet
p = fuel particles
r = reaction
ref = reference value
s = inert sand
surf = surface

REFERENCES

(1) Donald, L. K. *Biomass for Renewable Energy, Fuels, and Chemicals*; Academic Press: San Diego, 1998.

(2) McKendry, P. Energy production from biomass (part 2): conversion technologies. *Bioresour. Technol.* **2002**, *83*, 47–54.

(3) Kouprianov, V.; Permchart, W. Emissions from a conical FBC fired with biomass fuel. *Appl. Energy* **2003**, *74*, 383–392.

(4) Werther, J.; Saenger, M.; Hartge, E. U.; Ogada, T.; Siaga, Z. Combustion of agricultural residues. *Prog. Energy Combust. Sci.* **2000**, *26*, 1–27.

(5) Nemtsov, D. A.; Zabaniotou, A. Mathematical modelling and simulation approaches of agricultural residues air gasification in a bubbling fluidized bed reactor. *Chem. Eng. J.* **2008**, *143*, 10–31.

(6) Gómez-Barea, A.; Leckner, B. Modeling of biomass gasification in fluidized bed. *Prog. Energy Combust. Sci.* **2010**, *36*, 444–509.

(7) Kunii, D.; Levenspeil, O. *Fluidization Engineering*, 2nd ed.; Elsevier: Amsterdam, 1991.
(8) Davidson, J. F.; Harrison, D. *Fluidized Particles*; Cambridge University Press: Cambridge, U.K., 1963.
(9) Di Blasi, C. Modeling chemical and physical processes of wood and biomass pyrolysis. *Prog. Energy Combust. Sci.* **2008**, *19*, 47–90.
(10) Wiest, W. Zur Pyrolyse von Biomasse im Drehrohrreaktor. Ph.D. Dissertation, University of Kassel, Kassel, Germany, 1998.
(11) *DIN 51719: Determination of ash in solid mineral fuels*; Deutsches Institut für Normung (Hrsg.), Beuth Verlag: Berlin, 1997.
(12) *DIN 51720: Determing the volatile content of solid fuels*; Deutsches Institut für Normung (Hrsg.), Beuth Verlag: Berlin, 2001.
(13) Tepper, H. Zur Vergasung von Rest- und Abfallholz in Wirbelschichtreaktoren für Dezentrale Energieversorgungsanlagen. Ph.D. Thesis, Otto von Guericke University of Magdeburg, Magdeburg, Germany, 2005.
(14) Hobbs, M. L.; Radulovic, P. T.; Smoot, L. D. Modeling fixed-bed coal gasifiers. *AIChE J.* **1992**, *38*, 681–702.
(15) De Souza-Santos, M. L. Comprehensive modelling and simulation of fluidized bed boilers and gasifiers. *Fuel* **1989**, *68*, 1507–1521.
(16) Howard, J. B.; Williams, G. C.; Fine, D. H. Kinetics of carbon-monoxide oxidation in postflame gases. *Proc. Combust. Inst.* **1973**, *14*, 975–986.
(17) Chen, W. J.; Sheu, F. R.; Savage, R. L. Catalytic activity of coal ash on steam methane reforming and water−gas shift reactions. *Fuel Process. Technol.* **1987**, *16*, 279–288.
(18) Rumpel, S. Die autotherme Wirbelschichtpyrolyse zur Erzeugung heizwertreicher Stützbrennstoffe. Ph.D. Dissertation, Karlsruhe Institute of Technology, Karlsruhe, Germany, 2000.
(19) Jensen, A.; Johnsson, J. E.; Andreies, J.; Laughlin, K.; Read, G.; Mayer, M. Formation and reduction of NO_x in pressurized fluidized bed combustion of coal. *Fuel* **1995**, *74*, 1555–1569.
(20) Groenewold, H.; Tsotsas, E. Predicting Sherwood numbers in fluidised beds. *Drying Technol.* **1999**, *17*, 1557–1570.
(21) Gnielinski, V. Fluid−particle heat transfer in flow through packed bed of solids. In *VDI Heat Atlas*, 2nd ed.; Springer: Berlin, 2010; Section G9.
(22) Oka, S. N. *Fluidized Bed Combustion*; Marcel Dekker: New York, 2004.
(23) Kretschmer, F.; Surasani, V. K.; Bück, A.; Peglow, M.; Tsotsas, E. Particle size dependent devolatilization kinetics of biomass for a population balance model. Presented at the *ProcessNet Annual meeting on Gas Cleaning and High Temperature Technology*, Frankfurt am Main, Germany, Feb 17−18, 2011.
(24) Colaykan, M.; Levenspeiel, O. Elutriation from fluidized beds. *Powder Technol.* **1984**, *38*, 223–232.
(25) Wen, C. Y.; Chen, L. H. Fluidized bed freeboard phenomena: entrainment and elutriation. *AIChE J.* **1982**, *28*, 117–128.